

---

# Finding Patient Zero: Learning Contagion Source with Graph Neural Networks

---

Chintan Shah<sup>†1</sup>   Nima Dehmamy<sup>†2</sup>   Nicola Perra<sup>3</sup>   Matteo Chinazzi<sup>1</sup>  
Albert-László Barabási<sup>1,4</sup>   Alessandro Vespignani<sup>1</sup>   Rose Yu<sup>1,5\*</sup>

## Abstract

Locating the source of an epidemic, or patient zero (P0), can provide critical insights into the infection’s transmission course and allow efficient resource allocation. Existing methods use graph-theoretic centrality measures and expensive message-passing algorithms, requiring knowledge of the underlying dynamics and its parameters. In this paper, we revisit this problem using graph neural networks (GNNs) to learn P0. We establish a theoretical limit for the identification of P0 in a class of epidemic models. We evaluate our method against different epidemic models on both synthetic and a real-world contact network considering a disease with history and characteristics of COVID-19. We observe that GNNs can identify P0 close to the theoretical bound on accuracy, without explicit input of dynamics or its parameters. In addition, GNN is over 100 times faster than classic methods for inference on arbitrary graph topologies. Our theoretical bound also shows that the epidemic is like a ticking clock, emphasizing the importance of early contact-tracing. We find a maximum time after which accurate recovery of the source becomes impossible, regardless of the algorithm used.

## 1 Introduction

The ability to quickly identify the origin of an outbreak, or “finding patient zero”, is critically important in the effort to contain an emerging epidemic. The identification of early transmission chains and the reconstruction of the possible paths of diffusion of the virus can be the difference between stopping an outbreak in its infancy and letting an epidemic unfold and affect a large share of a population. Hence, solving this problem would be instrumental in informing and guiding contact tracing efforts carried out by public health authorities, allowing for optimal resource allocation that can maximize the probability of an early containment of the outbreak. Disease spreading is modeled as a *contagion process* on a network [42, 35] of human-to-human interactions where infected individuals are going to transmit the virus by infecting (with a certain probability) their direct contacts. In general, contagion processes can capture a wide range of phenomena, from rumor propagation on social media to virus spreading over cyber-physical networks [6, 2, 48, 31]. Therefore, learning the source of a contagion process would also have broader impact on various domains, from detecting sources of fake news to defending malware attacks.

Learning the *index case* (or P0) is a difficult problem. In this paper, we model disease spreading as a contagion process (chains of transmissions) over a graph. The evolution of an outbreak is noisy and highly dependent on the graph structure and disease dynamics. In addition, in real-world

---

<sup>†</sup> Equal contribution; Correspondence: shah.ch@husky.neu.edu, nima.dehmamy@kellogg.northwestern.edu, roseyu@eng.ucsd.edu <sup>1</sup>Northeastern University, Boston MA, USA, <sup>2</sup>Northwestern University, Evanston IL, USA, <sup>3</sup>Greenwich University, London, UK <sup>4</sup>Harvard University, Boston MA, USA, <sup>5</sup>University of California San Diego, USA.

epidemics, there is often a delay from the start of the outbreak to when epidemic surveillance and contact tracing starts. Hence, we might only observe the state of the graph at some intermediate times without access to the complete chains of transmission. Furthermore, due to its stochastic nature, the same source node might lead to different epidemic spreading trajectories. Finally, learning P0 from noisy observations of graph snapshots is computationally intractable and the complexity grows exponentially with the size of the graph [40].

Most work in learning the dynamics of a contagion process [38, 30, 23] have focused on inferring the *forward* dynamics of the diffusion. In epidemiology, for example, [36] have studied learning the temporal dynamics of diseases spreading on mobility networks. The problem of learning the *reverse* dynamics and identifying diffusion sources has been largely overlooked due to the aforementioned challenges. Two of the most notable exceptions in the area are “rumor centrality” [40] for contagion processes on trees and Dynamic Message-passing (DMP) on graphs [25] but both require as input the parameters of the spreading dynamics simulations.

Our goal is to provide fresh perspectives on the problem of finding *patient zero* using graph neural networks (GNNs) [14]. First, we conduct a rigorous analysis of learning P0 based on the graph structure and the disease dynamics, allowing us to find conditions for identifying P0 accurately. We test our theoretical results on a set of epidemic simulations on synthetic graphs commonly used in the literature [12, 1]. We also evaluate our method on a realistic co-location network for the greater Boston area, finding performance similar to the synthetic data. To the best of our knowledge, our work is the *first* to tackle the patient zero problem with deep learning and to test the approach on a realistic contact network. In summary, we make the following contributions:

- We find upper bounds on the accuracy of finding patient zero in graphs with cycles, independent of the inference algorithm used.
- We show that beyond a certain time scale the inference becomes difficult, highlighting the importance of swift and early contact-tracing.
- We demonstrate the superiority of GNNs over state-of-the-art message passing algorithms in terms of speed and accuracy. Most importantly, our method is model agnostic and does not require the epidemic parameters to be known.
- We validate our theoretical findings using extensive experiments for different epidemic dynamics and graph structures, including a real-world co-location graph of the COVID-19 outbreak.

## 2 Related Work

**Learning contagion dynamics** Learning forward dynamics of contagion processes on a graph is a well studied problem area. For instance, [38, 10] proposed scalable algorithms to estimate the parameters of the underlying diffusion network, a problem known as network inference. Deep learning has led to novel neural network models that can learn forward dynamics of various processes including neural Hawkes processes [30] and Markov decision processes-based reinforcement learning [23]. Learning forward contagion dynamics have also been intensively studied in epidemiology [36, 46], social science [27], and cyber-security [37]. In contrast, research in learning the reverse dynamics of contagion processes is rather scarce. Influence maximization [18], for instance, finds a small set of individuals that can effectively spread information in a graph, but only maximizes the number of affected nodes in the infinite time limit. Our problem is more difficult as we care not just about the number of infected nodes, but which nodes were infected.

**Finding patient zero** In order to find patient zero, we aim to learn the reverse dynamics of contagion processes. [40] were among the first to formalize the problem on trees in the context of modeling rumor spreading in a network. [37, 45] studied similar problems for detecting viruses in computer networks. [25] proposed a dynamic message passing algorithm to estimate the epidemic outbreak source. Fairly recently, [13] reduced the deanonymization of Bitcoin to the source identification problem in an epidemic and analyzes the dynamics properties. On the theoretical side, [40, 49] analyzed the quality of the maximum likelihood estimator and rumor centrality, but only for the simple SI model on trees. [20, 5] proved that it is possible to construct a confidence set for the predicted diffusion source nodes with a size independent of the number of infected nodes over a regular tree. Our work provides fresh perspectives on the patient zero problem on general graphs based on the recent development of graph neural networks

**Graph neural networks** Graph neural networks have received considerable attention (see several references in [4, 54, 51, 15]). While most research is focused on static graphs, a few have explored dynamic graphs [24, 53, 21, 34, 43]. For example, [21] propose a deep graph model to learn both the graph attribute and structure dynamics. They use a recurrent decoder to forecast the node attributes for multiple time steps ahead. [43] take a continuous-time modeling approach where they take the node embedding as the input and model the occurrence of an edge as a point process. [52] propose a temporal graph attention layer to learn the representations of temporal graphs. However, most research is designed for link prediction tasks and none of these existing studies have studied the problem of learning the source of the dynamics on a graph.

### 3 Contagion Process and Patient Zero

Finding patient zero means tracing the contagion dynamics back to its initial state and identifying the first nodes that started spreading. Here, we describe the disease dynamics on a network using Susceptible-Infected-Recovered (SIR) and Susceptible-Exposed-Infected-Recovered (SEIR) [19] compartmental models that assume that infected individuals develop immunity once they recover from the infections.

#### 3.1 Contagion processes on networks

In the SIR model, the population is split into three compartments: susceptible ( $S$ ) who are susceptible to infection by the disease; infected ( $I$ ) who have caught the disease and are infectious; removed ( $R$ ) who are removed from consideration after experiencing the full infectious period.

**Continuous time model** For a contagion process on a graph  $G$  with  $N$  nodes, each vertex represents an individual who is in contact only with its neighbors. We can represent the graph using the adjacency matrix  $A \in \mathbb{R}^{N \times N}$ , where  $A[i, j] = 1$  if two individuals are connected, 0 otherwise. Let  $S_i, I_i, R_i$  be the average probabilities of node  $i$  being in each of the states, with  $S_i + I_i + R_i = 1$ . The SIR dynamics on a graph is given by [33]:

$$\frac{dS_i}{dt} = -\beta \sum_j A_{ij} I_j S_i, \quad \frac{dR_i}{dt} = \gamma I_i, \quad \frac{dS_i}{dt} + \frac{dI_i}{dt} + \frac{dR_i}{dt} = 0. \quad (1)$$

where  $\beta$  is the infection rate per contact and  $\gamma$  the recovery/death rate. We can derive the rate of spreading given Eqn. (1). In early stages, when  $S_i \approx 1$ , the infection spreads as

$$I_i(t) \approx \sum_j \exp[t(\beta A - \gamma \mathbf{I})]_{ij} I_j(0) \approx \exp[(\beta \lambda_1 - \gamma)t] \left( \psi^{(1)} \cdot I(0) \right) \psi_i^{(1)}, \quad (2)$$

Here,  $\mathbf{I}$  is the identity matrix,  $\lambda_1$  is the largest eigenvalue of  $A$  and  $\psi^{(1)}$  is the corresponding eigenvector. The basic reproductive rate of a disease  $R_0 \equiv \beta \lambda_1 / \gamma$  is defined as the number of secondary infections created by an index case in a fully susceptible population [17]. The disease will spread and result in an epidemic if  $R_0 > 1$ .

**Discrete time model** We can also use an equivalent discrete time SIR model. Let  $x_i^t \in \{S, I, R\}$  be the state of node  $i$  at time  $t$ . For a susceptible node  $i$ , its probability to become infected or removed at time  $t + 1$  is

$$P(x_i^{t+1} = I | x_i^t = S) = 1 - \prod_j (1 - \beta A_{ij} I_j(t)), \quad P(x_i^{t+1} = R | x_i^t = I) = \gamma. \quad (3)$$

The SIR model doesn't account for the incubation period, where an individual is infected but not infectious. This is remedied by introducing an "exposed" (E) state, leading to the SEIR model. For a

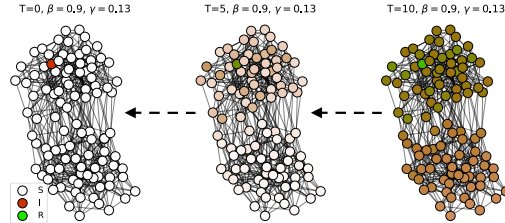


Figure 1: **Visualization of the patient zero problem:** uncover the original source (red node, left) given a future state of a contagion process (right).

susceptible node  $i$ , the probability to enter the exposed state, and becoming infectious at time  $t + 1$  is

$$P(x_i^{t+1} = E | x_i^t = S) = 1 - \prod_j (1 - \beta A_{ij} I_j(t)), \quad P(x_i^{t+1} = I | x_i^t = E) = \alpha, \quad (4)$$

An infected node eventually enters the removed state with probability  $\gamma$ , which is the same as SIR (3). (3) and (4) yield (1) for very small  $\beta$  as  $\prod_j (1 - \beta A_{ij} I_j) \approx \beta A_{ij} I_j$  (proof in supp. B).

**Finding patient zero** Finding P0 can be formulated as a maximum likelihood estimation problem for SIR and SEIR models. Specifically, we observe a snapshot of the state of the nodes at time step  $t$  as  $\mathbf{x}^t := (x_1^t, \dots, x_N^t)$ , with each node's state  $x_i^t \in \{S, E, I, R\}$ . The problem of finding P0 is to search for a set of nodes  $\mathcal{Z} = \{i | x_i^0 = I, i \in \{1, \dots, N\}\}$  which led to the observed state  $\mathbf{x}^t$ . A common approach is to find  $\mathcal{Z}$  such that the likelihood of observing  $\mathbf{x}^t$  is maximized:

$$\mathcal{Z}^* = \operatorname{argmax}_{\mathcal{Z}, |\mathcal{Z}| \leq k} P(\mathbf{x}^t | \mathcal{Z}) \quad (5)$$

where  $P(\mathbf{x}^t | \mathcal{Z})$  is the probability of observing  $\mathbf{x}^t$  with  $\mathcal{Z}$  being the P0 set. We assume the number of P0s is no larger than  $k$ . Estimating the original state of the dynamic system given the future states requires computing the conditional likelihood  $P(\mathbf{x}^t | \mathcal{Z})$  exactly, which is intractable due to the combinatorics of possible transmission routes.

### 3.2 Fundamental limit of finding patient zero

The technical difficulty of finding P0 in SIR and SEIR stems from: (1) presence of cycles in graphs (higher-order transmission) (2) the removed state introducing additional uncertainty about temporal order of infections (3) uncertainty of the exact time step of the observed states. For SI dynamics (i.e. infection is permanent) on trees, existing theoretical results [40, 20] have established upper bounds on the detection probability based on an estimator called ‘‘rumor centrality’’. For graphs with cycles, finding P0 becomes more elusive. We derive the fundamental limit considering the case where at time  $t = 0$  one node, P0, is infected and all of the other nodes are susceptible.

**Ambiguity of patient zero on cyclic graphs** For graph with cycles, if a cycle is embedded within the infected subgraph, it will reduce the accuracy of predicting P0 because multiple scenarios can lead to the same infection pattern in the cycle. For instance, take a 3-regular tree where the infection has started from the root and spread to some level. If we remove the root and instead connect the three children of the root as a triangle, the same infection pattern is possible with any of these three nodes being P0. Based on this observation, the following theorem estimates the time horizon beyond which finding P0 becomes difficult. We will focus on connected Erdős–Rényi (ER) random graphs [12], where each edge has probability  $p$ , independent of other edges.

**Theorem 1** (Time Horizon). *In a connected random graph, no algorithm can accurately detect P0 after  $t_{\max}$  time steps, approximately given by*

$$t_{\max} \sim \frac{\log N}{\gamma(R_0 - 1)} \quad (6)$$

*Proof:* The proof (supp. B.8.1) follows from (2) and setting  $\sum_i I_i(t_{\max}) \sim O(1)N$ .

The maximum detection accuracy of P0 on a connected ER would decrease when the infected subgraph contains cycles. We focus on triangles, as they are the most prevalent cycles in a random graph. We provide a conservative estimate assuming P0 is part of a triangle. This ignores cases where the presence of triangles causes downstream error or the error arising from other types of cycles. We derive an upper bound for the detection accuracy on a connected ER graph in the following theorem.

**Theorem 2** (Detection Accuracy). *In contagion process on a connected random graph  $G$ , with edge probability  $p$  and with infected subgraph  $G_I$ , the prediction accuracy for P0 is bounded from above*

$$P_{\max} < \frac{1}{3} + \frac{2}{3}(1-p)^{\binom{|G_I|}{2}p} \quad (7)$$

The proof (supp. B.8.2) follows from estimating number of triangles in subgraph  $G_I$  of a dense ER graph and noting each triangle can drop the accuracy of P0 to  $1/3$ .

Figure 2 shows an example of how this upper bound behaves for different values of  $R_0$ . The graph is a uniformly connected ER of  $N = 100$ ,  $p = 2 \log N/N$  and with  $\gamma = 0.4$ . In conclusion, on graphs with cycles, we expect finding P0 after a time  $t_{\max} \sim O(\log N)$  to become difficult. This suggests that to find P0 contact-tracing must be done promptly and in early stages.

## 4 Finding Patient Zero with Graph Neural Networks

We propose using GNNs for finding P0 and show that we can improve significantly upon state-of-the-art methods, e.g. DMP. Moreover, using GNNs gives us the distinct advantage that they are model-agnostic and do not require access to the epidemic dynamics parameters or the time  $t$  of the graph snapshot. Our goal is not to propose a novel graph neural network architecture, but to understand the trade-off between different probabilistic inference methods in the context of contagion dynamics. Before we discuss our GNN solution, we briefly review Dynamic Message Passing.

**Dynamic Message Passing** DMP [25] estimates the probability of every node being the P0 in the SIR model using message-passing equations and approximates the joint likelihood with a mean-field time approach by assuming the following factorization:

$$P(\mathbf{x}^t|\mathcal{Z}) \approx \prod_{i, x_i^t=S} P(x_i^t|\mathcal{Z}) \prod_{j, x_j^t=I} P(x_j^t|\mathcal{Z}) \prod_{k, x_k^t=R} P(x_k^t|\mathcal{Z}) \quad (8)$$

The algorithmic complexity of the DMP equations over a graph with  $N$  nodes and  $t \leq T$  diffusion steps is  $O(TN^2\langle k \rangle)$  where  $\langle k \rangle$  is the average degree of the graph. Furthermore, DMP requires providing the SIR epidemic parameters and the time  $t$  of the graph snapshot before performing inference. For comparison, on a connected random graph,  $\langle k \rangle > \log N$ , yielding  $> O(TN^2 \log N)$  time complexity for DMP. A trained GNN with  $l \sim \text{Dia}(G) \sim \log N$  layers has complexity  $O(N^2 \log N)$  in the inference step and does not require inputting the model parameters. This makes it harder to scale DMP for large or dense graphs. DMP is proven to be exact on trees, e.g. [16], and has been used on more general graphs with reasonable success.

**Relation between Contagion Dynamics and GNNs** Our use of GNNs for finding P0 is motivated by the fact that the contagion dynamics (1) are a special case of Reaction-Diffusion (RD) processes on graphs [8] which is structurally equivalent to GNNs, as shown in the following proposition.

**Proposition 1.** *Reaction-diffusion dynamics on graphs is structurally equivalent to the message-passing neural network ansatz.*

Denoting  $p_i^\mu(t) \equiv P(x_i^t = \mu)$  of node  $i$  being in states such as  $\mu \in \{S, I, R\}$  or  $\mu \in \{S, E, I, R\}$  at time  $t$ , a Markovian reaction-diffusion dynamics can be written as

$$p_i^\mu(t+1) = \sigma \left( \sum_j F(\mathcal{A}_{ij} \cdot h(p_j)^\mu) \right), \quad h_a(p_i)^\mu = \sigma \left( \sum_\nu W_{a,\nu}^\mu p_i^\nu + b^\mu \right) \quad (9)$$

where  $\mathcal{A}_{ij}^a = \theta(A_{ij})f(A)_{ij}$  with  $\theta(\cdot)$  being the step function and  $\sigma(\cdot)$  a nonlinear function. RD on graphs is structurally equivalent to Message-passing Neural Networks (MPNN) [14], as RD involves a message-passing step and a node-wise interaction among features (Supp. B.3), same as MPNN. We choose the simpler architecture of GCN as in (10) instead of general MPNN. Finding P0 requires learning the backward dynamics of RD, which seems to require the inverse of the propagation rule (PR). Yet, each node can only get infected by its neighbors, so even the backward dynamics requires message passing over the same adjacency matrix and should again have the structure of RD.

### 4.1 Learning with Graph Neural Networks

We employ a state-of-the-art GNN design, suggested by [11]. We make several modifications to the model architecture to fit our problem. Given one-hot encoded node states  $x_i^t \in \{0, 1\}^M$  as the GNN input, where  $M$  is the number of states and where the states are either  $\{S, E, I, R\}$  or  $\{S, I, R\}$ , we first apply a linear transformation  $h_i^{(0)} = Ux_i^t$  with  $U \in \mathbb{R}^{C \times M}$ . Denote the output of layer  $l$  by  $h_i^{(l)}$ , where  $i$  is the node index. We use graph convolutional network (GCN) [22] in each layer  $g(h) = \sigma_g(f(A) \cdot h \cdot W + b)$ , where  $W \in \mathbb{R}^{C \times C}$ ,  $b \in \mathbb{R}^C$  and  $f$  is called the propagation rule in GCN. We use  $f(A) = D^{-1/2}AD^{-1/2}$  for the propagation rule, where  $D_{ij} = \delta_{ij} \sum_k A_{ik}$  is the degree matrix. To include features of the central node, instead of adding self-loops, we use residual connections between GCN layers and notice a significant increase in model performance. The action of these higher GNN layers can be summarized as

$$h_i^{(l+1)} = h_i^{(l)} + \sigma \left( \text{BN}(g(h_i^{(l)})) \right), \quad y_i = P \cdot \text{ReLU}(Q \cdot h_i^{(L)}) \quad (10)$$

where  $L$  is the number of layers and the output layer is parameterized by  $Q \in \mathbb{R}^{D \times D}$  and  $P \in \mathbb{R}^{1 \times D}$  to generate  $y_i \in \mathbb{R}$ , representing the probability that node  $i$  is P0.  $\text{BN}(\cdot)$  denotes Batch Normalization and  $\sigma(\cdot)$  is a leaky-relu nonlinear activation function.

**Architecture design guideline** Using GNN to find P0 requires designing the appropriate neural network architecture. The following proposition provides a guideline on choosing the depth of a GNN based on the diameter of the underlying graph.

**Proposition 2.** *In the worst case, after  $\tau$  steps of RD dynamics on a graph with diameter  $\text{Dia}(G)$ , we need  $l_{MP} > \min(\tau, \text{Dia}(G))$  layers of message-passing (MP) to be able to identify all P0.*

See supp. B.7 for proof. The intuition is that, each MP step can incorporate neighbors one more step away. Since after  $\tau$  steps P0 and the last infected nodes can be upto  $\text{Dia}(G)$  steps apart, any GNN architecture doesn't need to be much deeper than the diameter of the graph. Random graphs generally have very short diameters, around  $\text{Dia}(G) \sim \log N$ , but geometric graphs, such as the Random Geometric Graph (RGG), where nodes connect to nodes close-by, have larger diameters roughly  $\text{Dia}(G) \sim N^{1/d}$  where  $d$  is the dimensions of the space. For example, if there are no long-distance travels, the contact network of people in a town or city is roughly an RGG in 2D.

## 5 Experiments

We perform extensive studies on performance of our GCNs in finding P0 in SIR and SEIR dynamics over synthetic graphs with various graph topologies. In addition, we generate synthetic epidemic outbreaks on top of a real world co-location network using a SEIR compartmental model that is calibrated to simulate a contagion process with characteristics similar to a COVID-19 outbreak.

**Experimental Setup** We compare the performance of DMP [25] and different variants of GCNs, following the architecture we described in sec. 4.1:

- DMP: Dynamic Message Passing algorithm [25], we sample a graph snapshot  $O$  at time  $t$  with each node having a state  $x_i^t \in \{S, I, R\}$ , and select the node  $i$  that has the highest likelihood of generating  $O$ , that is  $\text{P0} = \arg\max_i P(O|x_i^0 = I)$ .
- GCN-S: symmetric GCN [22]  $f(A) = D^{1/2}AD^{1/2}$ , GCN-R: random walk  $f(A) = D^{-1}A$ , GCN-M: mixture of propagation rules  $f(A) = A||D^{1/2}AD^{1/2}$
- GAT: Graph Attention Network [44]

We train our models using DGL [47] with a PyTorch backend. The task is to predict the probability for each node being P0 given a single graph snapshot. We train the model with an ADAM optimizer for 150 epochs with an initial learning rate of 0.003 and decay the learning rate by 0.5 when the validation loss plateaus with a patience of 10 epochs. We perform hyperparameter tuning over a validation set with a random search strategy. We sweep over the hyperparameter space and track our experiments using Weights and Biases [3] choosing the model with the lowest validation error. We run our experiments on Nvidia 2080Ti GPUs and report performance averaged over 4 random seeds. We additionally report inference run times.

**Evaluation Metrics** We use top-1 accuracy to understand the effectiveness of our method. However, due to the ambiguity of detecting patient zero, as elaborated in our theoretical analysis, top-1 accuracy may not be the only evaluation measure to be relied upon. Therefore we also calculate the normalized rank defined by  $R_t = 1 - \frac{1}{|D_t|N} \sum_{u \in D_t} r_u$  where  $D_t$  is the set of test samples at time  $t$ ,  $N$  is the size of the graph and  $r_u$  is the index of the ground truth P0 in the reverse-sorted probability distribution. Normalized rank is a retrieval metric that tells us how high the correct patient zero was in the learned output distribution. It demonstrates the quality of the output distribution in learning the stochastic dynamics and helps us understand how high was P0 ranked even if it was not ranked the first.

### 5.1 Experiments with Synthetic Networks

We use three graph models: ER random graph, Barabási-Albert (BA) graph [1] and Random Geometric Graph (Geometric or RGG) [9]. The density of all three ( $|E|/\binom{N}{2}$ ) is adjustable, but BA can

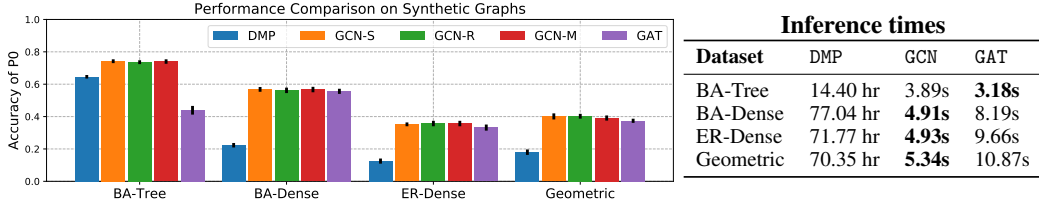


Figure 3: Mean Prediction accuracy/speed comparison for different methods for the test set over  $T = 30$  steps and  $R_0 = 2.5$ . The time to perform inference over the test set for different models have been listed above. Note that the time taken by GCN represents the mean time taken by GCN variants. We observe that GNNs beat DMP by a large margin both in terms of speed and accuracy.

produce exact trees. Fixing the number of nodes to  $N = 1,000$ , we first obtain one random instance of tree BA, and dense BA, ER and Geometric graphs with  $|E| \approx 10,000$  using the NetworkX library [32] and then use NDLiB [39] to simulate SIR and SEIR epidemic dynamics on the graph (supp. A.1). For each sample graph, we pick a P0 seed node  $i$  at random to be the patient zero at time  $t = 0$  and then we run S(E)IR a fixed number of steps  $T$ . The epidemic parameters  $(\alpha, \beta, \gamma)$  are chosen such that we can vary  $R_0$  to study model performance. We set  $\gamma = 0.4$  and  $\beta = R_0\gamma/\lambda_1$  where  $\lambda_1$  is the largest eigenvalue of the graph. For SEIR, we set  $\alpha = 0.5$ . We generate 20,000 simulations and use 80 – 10 – 10 train-validation-test split. For each sample we select  $t \in \{1, \dots, T\}$  uniformly at random and try to predict P0 at time  $t = 0$  given the graph adjacency matrix  $A$  and node features  $x_i^t$ .

We first compare the top-1 prediction accuracy in SIR and SEIR for different models averaged over  $1 \leq t \leq T$ . Fig 3 compares the prediction accuracy and average inference time for different models. We can see that GNN-based models outperform the baseline DMP both in accuracy and efficiency. We also want to note that the training time for GNNs is under 7 hours, significantly less than the fastest DMP run of 14.40 hr. It is also worth emphasizing that DMP requires explicit input of  $\beta, \gamma$  and  $t$  while GNNs are model agnostic.

To validate our theory, we plot the theoretical accuracy upper-bound and the empirical accuracy obtained from GNN in Fig. 2. We note that the time scale and amount of drops are consistent with our theoretical results on  $t_{\max}$  (6) and the upper bound on accuracy  $P_{\max}$  (7). Combined with the fact that all our GNN models have comparable accuracies, this suggests that our GCN-based models may be approaching the fundamental limits we described in 3.2.

Fig. 4 shows the trend of accuracy decay over the time steps  $t$  for different graph structures and  $R_0$  values. As expected, the accuracy is highest on a tree and when  $t$  is small. In graphs with cycles (BA-Dense, ER-Dense, and Geometric) we also observe a nontrivial drop in accuracy which depends both on  $t$  and  $R_0$ . For SIR we observe a drop in accuracy as a function of  $R_0$  and time, consistent with our theoretical upper bound. The decay is slower for SEIR as the latent stage adds a delay to the spread of the epidemic. The normalized rank of P0 remains high even over longer time horizons, indicating that P0 could be narrowed down to small subset of the population with impressive accuracy.

## 5.2 Experiments with Boston co-location network and COVID-19 epidemic trajectory

Our real-world dataset consists of a co-location graph and simulations of an epidemic with the natural progression of COVID-19. The co-location graph is constructed using the Cuebiq data (<https://www.cuebiq.com/about/data-for-good/>) for two weeks from 23 March, 2020 to 5 April, 2020 ( $N = 384,590$  nodes). To reduce computational costs, we sample a subgraph with  $N = 2,689$  nodes and  $|E| = 30,376$  edges while maintaining the degree distribution and connectivity patterns of the original graph. For the epidemic simulations, we run a modified SEIR model with

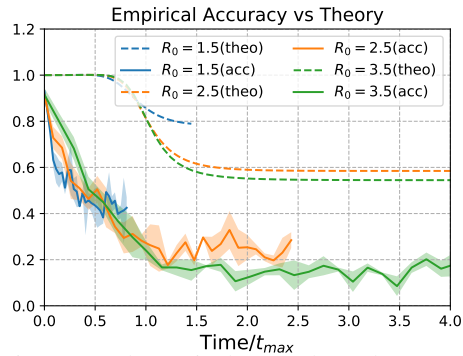


Figure 2: Theoretical upper bound on accuracy (dashed line) vs experimental (solid line) on ER for varying  $R_0$ . While accuracy drops below the theoretical limit at  $t \sim t_{\max}$ .

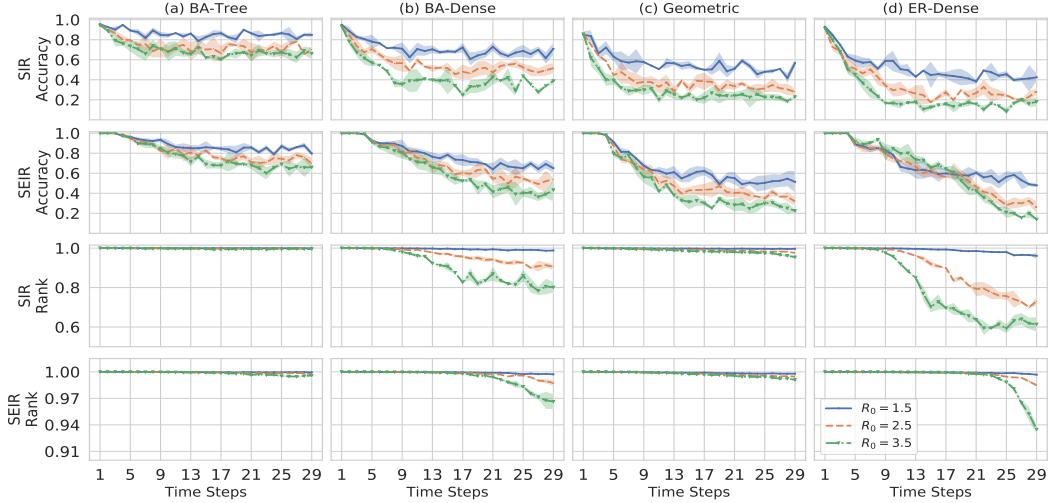


Figure 4: Performance of GCN-S for SIR and SEIR epidemic dynamics as top-1 accuracy over the test set. The top-1 recovery accuracy of P0 vs time (first and second row) and normalized rank of P0 (third and fourth row) for different graph topologies with varying  $R_0$  values. Note that in BA-Tree (a), which is a tree, the accuracy remains fairly high in both SIR and SEIR, consistent with existing literature, and confirming that cycles significantly reduces accuracy of P0. Performance as normalized rank over the test set indicates that P0 can be narrowed down to a small subset of the population.

asymptomatic infectious states on the co-location graph with  $R_0$  resembling COVID-19 [7] and accordingly set  $R_0 = 2.5$ . Each simulation contains 1 patient zero, selected uniformly at random. The simulation is run for 50 days. We create a dataset with 10,000 samples and an 80 – 10 – 10 train-validation-test split (supp. C).

The top-k accuracy performance over different days when the graph snapshot was observed are shown in Fig. 5a. We can see that the top-1 accuracy falls steadily over time, the top-(10, 20) accuracy remains fairly high for the first two weeks suggesting that we can retrieve P0 in the most likely 20 nodes out of a total 2,689 candidates.

Interesting, while the top-1 accuracy decreases significantly, degrading by 50% after 14 days, using normalized rank, the model can narrow down the set of patient zeros accurately even later in the epidemic, as shown in Fig 5b. For the normalized rank, P0 can be recovered fairly accurately in the first two weeks of the epidemic. These results highlight an important trade-off between accurately determining patient zero and retrieving the general infected region.

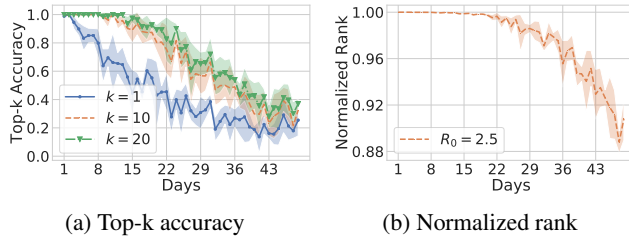


Figure 5: Performance on Boston co-location network with simulations following the natural history of COVID-19. Shown here are the top-k accuracy and normalized rank.

## 6 Conclusion

We study contagion dynamics on a graph using graph neural networks (GNNs) to learn the reverse dynamics of contagion processes and predict patient zero. We evaluate our method against different epidemic models on both synthetic and a real-world contact network with a disease with the natural history and characteristics of COVID-19. We observe that GNNs can efficiently infer the source of an outbreak without explicit input of dynamics parameters. Most notably, GNN accuracy approaches our predicted theoretical upper bound, indicating that further architecture refinements may not improve performance significantly. In addition, GNN is over 100x faster for inference than classic methods for arbitrary graph topologies. Extensions of this work may include learning using sequences of graph snapshots, as well as allowing a set of patient zeros.



## Broader Impact

This work will have a direct impact on improving societal resilience against epidemics, introducing new computational tools to disease modeling, and informing and educating about the science of virus transmission and prevention. Misuse of our research can lead to political biases and legitimizing conspiracy theories of disease origin. The other ethical challenge of our framework is data privacy. The mobility data used in this study – provided by Cuebiq through its Data for Good program (<https://www.cuebiq.com/about/data-for-good/>) – are aggregated and privacy-enhanced mobility data for academic research and humanitarian initiatives. These first-party data are collected from users who have opted in to provide access to their GPS location data anonymously, through a GDPR-compliant framework. Furthermore, in our analysis the geospatial information is used only to create a series of co-location events that are used as proxy for human-to-human contacts. Geolocation information is not actually used to conduct the research and no user-sensitive information is available to us. On the technical side, our work highlights an aspect of graph neural networks which has been largely ignored, namely whether or not certain inference problems on graphs are at all information-theoretically possible. We find that in a general class of dynamic problems on graphs, including epidemics and spreading of news or misinformation, finding the source requires prompt action and that past a certain time it will be exceedingly difficult to find the source.

## References

- [1] Réka Albert and Albert-László Barabási. Statistical mechanics of complex networks. *Reviews of modern physics*, 74(1):47, 2002.
- [2] Andrea Baronchelli. The emergence of consensus: a primer. *Royal Society open science*, 5(2):172189, 2018.
- [3] Lukas Biewald. Experiment tracking with weights and biases, 2020. Software available from wandb.com.
- [4] Michael M Bronstein, Joan Bruna, Yann LeCun, Arthur Szlam, and Pierre Vandergheynst. Geometric deep learning: going beyond euclidean data. *IEEE Signal Processing Magazine*, 34(4):18–42, 2017.
- [5] Sébastien Bubeck, Luc Devroye, and Gábor Lugosi. Finding adam in random growing trees. *Random Structures & Algorithms*, 50(2):158–172, 2017.
- [6] Damon Centola and Michael Macy. Complex contagions and the weakness of long ties. *American journal of Sociology*, 113(3):702–734, 2007.
- [7] Matteo Chinazzi, Jessica T. Davis, Marco Ajelli, Corrado Gioannini, Maria Litvinova, Stefano Merler, Ana Pastore y Piontti, Kunpeng Mu, Luca Rossi, Kaiyuan Sun, Cécile Viboud, Xinyue Xiong, Hongjie Yu, M. Elizabeth Halloran, Ira M. Longini, and Alessandro Vespignani. The effect of travel restrictions on the spread of the 2019 novel coronavirus (covid-19) outbreak. *Science*, 368(6489):395–400, 2020.
- [8] Vittoria Colizza, Romualdo Pastor-Satorras, and Alessandro Vespignani. Reaction–diffusion processes and metapopulation models in heterogeneous networks. *Nature Physics*, 3(4):276–282, 2007.
- [9] Jesper Dall and Michael Christensen. Random geometric graphs. *Physical review E*, 66(1):016121, 2002.
- [10] Nan Du, Le Song, Manuel Gomez Rodriguez, and Hongyuan Zha. Scalable influence estimation in continuous-time diffusion networks. In *Advances in neural information processing systems*, pages 3147–3155, 2013.
- [11] Vijay Prakash Dwivedi, Chaitanya K. Joshi, Thomas Laurent, Yoshua Bengio, and Xavier Bresson. Benchmarking graph neural networks, 2020.
- [12] Paul Erdős, Alfréd Rényi, et al. On random graphs. *Publicationes mathematicae*, 6(26):290–297, 1959.
- [13] Giulia Fanti and Pramod Viswanath. Deanonimization in the bitcoin p2p network. In *Advances in Neural Information Processing Systems*, pages 1364–1373, 2017.
- [14] Justin Gilmer, Samuel S Schoenholz, Patrick F Riley, Oriol Vinyals, and George E Dahl. Neural message passing for quantum chemistry. In *Proceedings of the 34th International Conference on Machine Learning—Volume 70*, pages 1263–1272. JMLR. org, 2017.
- [15] Palash Goyal and Emilio Ferrara. Graph embedding techniques, applications, and performance: A survey. *Knowledge-Based Systems*, 151:78–94, 2018.
- [16] Yashodhan Kanoria, Andrea Montanari, et al. Majority dynamics on trees and the dynamic cavity method. *The Annals of Applied Probability*, 21(5):1694–1748, 2011.
- [17] Matt J Keeling and Pejman Rohani. *Modeling infectious diseases in humans and animals*. Princeton University Press, 2011.

- [18] David Kempe, Jon Kleinberg, and Éva Tardos. Maximizing the spread of influence through a social network. In *Proceedings of the ninth ACM SIGKDD international conference on Knowledge discovery and data mining*, pages 137–146, 2003.
- [19] William Ogilvy Kermack and Anderson G McKendrick. A contribution to the mathematical theory of epidemics. *Proceedings of the royal society of london. Series A, Containing papers of a mathematical and physical character*, 115(772):700–721, 1927.
- [20] Justin Khim and Po-Ling Loh. Confidence sets for the source of a diffusion in regular trees. *IEEE Transactions on Network Science and Engineering*, 4(1):27–40, 2016.
- [21] Thomas Kipf, Ethan Fetaya, Kuan-Chieh Wang, Max Welling, and Richard Zemel. Neural relational inference for interacting systems. *arXiv preprint arXiv:1802.04687*, 2018.
- [22] Thomas N Kipf and Max Welling. Semi-supervised classification with graph convolutional networks. *arXiv preprint arXiv:1609.02907*, 2016.
- [23] Shuang Li, Shuai Xiao, Shixiang Zhu, Nan Du, Yao Xie, and Le Song. Learning temporal point processes via reinforcement learning. In *Advances in neural information processing systems*, pages 10781–10791, 2018.
- [24] Yaguang Li, Rose Yu, Cyrus Shahabi, and Yan Liu. Diffusion convolutional recurrent neural network: Data-driven traffic forecasting. In *International Conference on Learning Representations (ICLR)*, 2018.
- [25] Andrey Y Lokhov, Marc Mézard, Hiroki Ohta, and Lenka Zdeborová. Inferring the origin of an epidemic with a dynamic message-passing algorithm. *Physical Review E*, 90(1):012801, 2014.
- [26] Naoki Masuda and Petter Holme. *Temporal network epidemiology*. Springer, 2017.
- [27] Yasuko Matsubara, Yasushi Sakurai, B Aditya Prakash, Lei Li, and Christos Faloutsos. Rise and fall patterns of information diffusion: model and implications. In *Proceedings of the 18th ACM SIGKDD international conference on Knowledge discovery and data mining*, pages 6–14, 2012.
- [28] Brendan D McKay et al. *Practical graph isomorphism*. Department of Computer Science, Vanderbilt University Tennessee, USA, 1981.
- [29] Brendan D. McKay and Adolfo Piperno. Practical graph isomorphism, ii. *Journal of Symbolic Computation*, 60:94 – 112, 2014.
- [30] Hongyuan Mei and Jason M Eisner. The neural hawkes process: A neurally self-modulating multivariate point process. In *Advances in Neural Information Processing Systems*, pages 6754–6764, 2017.
- [31] Bimal Kumar Mishra and Neha Keshri. Mathematical model on the transmission of worms in wireless sensor network. *Applied Mathematical Modelling*, 37(6):4103–4111, 2013.
- [32] NetworkX developer team. *Networkx*, 2014.
- [33] Mark Newman. *Networks: an introduction*. Oxford university press, 2018.
- [34] Aldo Pareja, Giacomo Domeniconi, Jie Chen, Tengfei Ma, Toyotaro Suzumura, Hiroki Kanezashi, Tim Kaler, and Charles E Leiserson. Evolvegen: Evolving graph convolutional networks for dynamic graphs. *arXiv preprint arXiv:1902.10191*, 2019.
- [35] Romualdo Pastor-Satorras, Claudio Castellano, Piet Van Mieghem, and Alessandro Vespignani. Epidemic processes in complex networks. *Reviews of modern physics*, 87(3):925, 2015.
- [36] Romualdo Pastor-Satorras and Alessandro Vespignani. Epidemic spreading in scale-free networks. *Physical review letters*, 86(14):3200, 2001.
- [37] B Aditya Prakash, Jilles Vreeken, and Christos Faloutsos. Spotting culprits in epidemics: How many and which ones? In *2012 IEEE 12th International Conference on Data Mining*, pages 11–20. IEEE, 2012.
- [38] Manuel Gomez Rodriguez, David Balduzzi, and Bernhard Schölkopf. *Uncovering the temporal dynamics of diffusion networks*. 2011.
- [39] Giulio Rossetti, Letizia Milli, Salvatore Rinzivillo, Alina Sirbu, Dino Pedreschi, and Fosca Giannotti. Ndlb: a python library to model and analyze diffusion processes over complex networks. *International Journal of Data Science and Analytics*, 5(1):61–79, Dec 2017.
- [40] Devavrat Shah and Tauhid Zaman. Rumors in a network: Who’s the culprit? *IEEE Transactions on information theory*, 57(8):5163–5181, 2011.
- [41] Nino Shervashidze, Pascal Schweitzer, Erik Jan van Leeuwen, Kurt Mehlhorn, and Karsten M Borgwardt. Weisfeiler-lehman graph kernels. *Journal of Machine Learning Research*, 12(Sep):2539–2561, 2011.
- [42] Daniel W Stroock and SR Srinivasa Varadhan. *Multidimensional diffusion processes*. Springer, 2007.
- [43] Rakshit Trivedi, Mehrdad Farajtabar, Prasenjeet Biswal, and Hongyuan Zha. Dyrep: Learning representations over dynamic graphs. In *International Conference on Learning Representations*, 2019.

- [44] Petar Veličković, Guillem Cucurull, Arantxa Casanova, Adriana Romero, Pietro Lio, and Yoshua Bengio. Graph attention networks. *arXiv preprint arXiv:1710.10903*, 2017.
- [45] Soroush Vosoughi, Mostafa ‘Neo’ Mohsenvand, and Deb Roy. Rumor gauge: Predicting the veracity of rumors on twitter. *ACM transactions on knowledge discovery from data (TKDD)*, 11(4):1–36, 2017.
- [46] Emilia Vynnycky and Richard White. *An introduction to infectious disease modelling*. OUP oxford, 2010.
- [47] Minjie Wang, Lingfan Yu, Da Zheng, Quan Gan, Yu Gai, Zihao Ye, Mufei Li, Jinjing Zhou, Qi Huang, Chao Ma, Ziyue Huang, Qipeng Guo, Hao Zhang, Haibin Lin, Junbo Zhao, Jinyang Li, Alexander J Smola, and Zheng Zhang. Deep graph library: Towards efficient and scalable deep learning on graphs. *ICLR Workshop on Representation Learning on Graphs and Manifolds*, 2019.
- [48] Yini Wang, Sheng Wen, Yang Xiang, and Wanlei Zhou. Modeling the propagation of worms in networks: A survey. *IEEE Communications Surveys & Tutorials*, 16(2):942–960, 2013.
- [49] Zhaoxu Wang, Wenxiang Dong, Wenyi Zhang, and Chee Wei Tan. Rumor source detection with multiple observations: Fundamental limits and algorithms. *ACM SIGMETRICS Performance Evaluation Review*, 42(1):1–13, 2014.
- [50] Boris Weisfeiler and Andrei A Lehman. A reduction of a graph to a canonical form and an algebra arising during this reduction. *Nauchno-Technicheskaya Informatsia*, 2(9):12–16, 1968.
- [51] Zonghan Wu, Shirui Pan, Fengwen Chen, Guodong Long, Chengqi Zhang, and Philip S Yu. A comprehensive survey on graph neural networks. *arXiv preprint arXiv:1901.00596*, 2019.
- [52] Da Xu, Chuanwei Ruan, Evren Korpeoglu, Sushant Kumar, and Kannan Achan. Inductive representation learning on temporal graphs. *arXiv preprint arXiv:2002.07962*, 2020.
- [53] Jiaxuan You, Bowen Liu, Rex Ying, Vijay Pande, and Jure Leskovec. Graph convolutional policy network for goal-directed molecular graph generation. *arXiv preprint arXiv:1806.02473*, 2018.
- [54] Ziwei Zhang, Peng Cui, and Wenwu Zhu. Deep learning on graphs: A survey. *arXiv preprint arXiv:1812.04202*, 2018.

## A Appendix

### A.1 Dataset Details

Table 1 describes the details of the synthetic datasets.

Table 1: Description of the sampled graph statistics

Dataset	# of Nodes	# of Edges	Density	Diameter
BA-Tree	1,000	999	0.99	19
BA-Dense	1,000	9,900	9.90	4
Geometric	1,000	9,282	9.28	21
ER-Dense	1,000	9,930	9.93	4

### A.2 Hyper-parameter Details

Table 2: Description of hyper-parameters used. All of our models have been trained with 4 random seeds. The initial learning rate is mentioned in the table below and additionally we decay the learning rate by 0.5 with a patience of 10 epochs when the validation error plateaus. Note that GAT had 4 attention heads and has been trained with 5 layers due to a limitation on GPU memory.

Hyperparameters	GCN-S	GCN-R	GCN-M	GAT
Number of Epochs	150	150	150	150
Batch Size	128	128	128	32
GNN Hidden Dim	128	128	128	128
Dropout	0.265	0.265	0.265	0.265
Number of GNN Layers	10	10	10	5
Initial Learning Rate	0.0033	0.0033	0.0033	0.004

### A.3 Notes on DMP implementation

We include DMP [25] as a baseline against our proposed GNN based method. As DMP does not have code that is publicly available, we implemented DMP using Python for a fair comparison with GNNs. Accordingly, our implementation of DMP uses DGL [47] which enables us to vectorize belief propagation (BP) and marginalization and now it runs in parallel for all nodes.

Given a graph  $G(V, E)$ , we observe  $O^t$  as the state of the graph with nodes  $i \in V$ . DMP employs MLE estimation to determine the node  $i_{P0}$  that may have led to the observed snapshot  $O$ . For a single sample in our dataset  $D$ , we use algorithm 1. In order to implement DMP efficiently, we implemented it as a message-passing on a graph using DGL. We sequentially initialize node and edge features for all node  $i$  and then as we obtain  $N = |V|$  set of graphs with node  $i$  acting as P0 in  $G_i$ . DMP then allows us to obtain  $i = \operatorname{argmax}_i P(O|i)$ . The advantage of our implementation then is that we can process all  $N$  graphs in parallel as if it were one large graph with  $N^2$  nodes and  $E^2$  edges thanks to DGL’s support for batching graphs. A salient feature of using DGL is that the message passing framework allows us to additionally process all the nodes and edges for a single time step  $t$  in parallel. The nature of BP algorithms do not allow us to do away with the for-loop over time  $t$  and that remains the only sequential aspect of our implementation. Finally, we use algorithm 1 to process each sample in our test set sequentially. It should be noted that we can further vectorize over a batch of samples in our test

set. However, the memory required for DMP is  $O(bN^2E^2)$  with  $b$  being the size of the batch and so memory requirements quickly blow up. Accordingly, we leave this aspect of implementation for future work.

---

**Algorithm 1:** Dynamic Message Passing given graph  $G$ , snapshot  $O$  and time  $t$

---

```

for  $i \in V$  do
  set node  $i$  to be P0
  initialize node features and edge features with eq (12, 13) in DMP;
  for ( $t = 0$ ;  $t < \mathbf{t}$ ;  $t = t + 1$ ) do
    for  $e \in E$  do
      perform message passing with eq (15, 16, 17) in DMP
    for  $j \in V$  do
      marginalize and update node states with eq (18, 19, 20) in DMP.
    Calculate  $P(O|i)$  with eq 21 in DMP.
return  $i = \operatorname{argmax}_i P(O|i)$ 

```

---

#### A.4 Effect of varying number of GCN-S layers on top-1 accuracy

Fig. 6 shows the top-1 accuracy of P0 of the GCN-S model for varying number of layers. We do not observe a significant effect coming from the number of layers. This may be due to the accuracy limitations with  $t_{\max}$  and cycles affecting all the models equally, and superseding other effects such as the diameter of the graph. Another possible reason may be that the 20,000 samples on a graph of 1,000 nodes has many repetitions of the same P0, resulting in both shallow and deep models memorizing patterns.

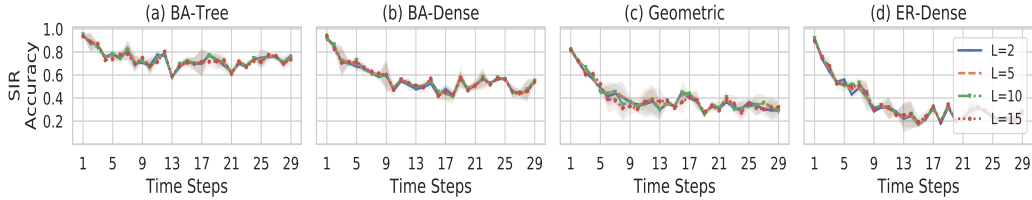


Figure 6: Performance of GCN-S for SIR epidemic dynamics as top-1 accuracy over the test set with varying number of layers.

## B Theoretical Analysis

### B.1 Early Stage Evolution of SIR and SEIR

The SIR equation on a graph are

$$\frac{dS_i}{dt} = -\beta \sum_j A_{ij} I_j S_i, \quad \frac{dR_i}{dt} = \gamma I_i, \quad \frac{dS_i}{dt} + \frac{dI_i}{dt} + \frac{dR_i}{dt} = 0. \quad (11)$$

In very early stages, when  $t \ll 1/\gamma$  and  $\sum_i I_i + R_i \ll N$ , we have  $S_i \approx 1$  and we have exponential for  $I_i$  because

$$\begin{aligned} \frac{dI_i}{dt} &= \beta \sum_j A_{ij} I_j S_i - \gamma I_i \approx \sum_j (\beta A_{ij} - \gamma \delta_{ij}) I_j \\ I_i(t) &\approx \sum_j (\exp[t(\beta A - \gamma \mathbf{I})])_{ij} I_j(0) \end{aligned} \quad (12)$$

Expanding this using the eigen-decomposition  $A = \sum_i \lambda_i \psi_i \psi_i^T$  yields eq. (2).

### B.2 Transition Probabilities

More generally, when the graph is weighted, the probability of susceptible node  $i$  getting infected depends on  $A_{ij}$  and the probability of node  $j$  being in the infected state. For brevity, define  $p_i^\mu(t) \equiv P(x_i^t = \mu)$ , with  $\mu \in \{S, I, \dots, R\}$ . The infection probability in SIR (3) can be written as

$$P(x_i^{t+1} = I | x_i^t = S) = 1 - \prod_j (1 - \beta A_{ij} p_j^I) = \beta \sum_j A_{ij} p_j^I - \beta^2 [A p^I]^2 + O(\beta^3). \quad (13)$$

### B.3 Reaction Diffusion Formulation

For brevity, define  $p_i^\mu(t) \equiv P(x_i^t = \mu)$ . In a network diffusion process the assumption is that node  $i$  can only be directly affected by state of node  $j$  if there is a connection between them, i.e. if  $A_{ij} \neq 0$ . This restriction means that the general reaction-diffusion process on a graph has the form

$$F_a(A; p)_i^\mu \equiv \sum_j f_a(g_a(A)_{ij} h_a(p_j)^\mu) \quad (14)$$

$$p_i^\mu(t+1) = F(A; p(t))_i^\mu = \sigma(\{F_a(A; p(t))_i^\mu\}) \quad (15)$$

With

$$g_a(A)_{ij} = \theta(A_{ij}) \tilde{g}_a(A)_{ij} \quad h_a(p_i)^\mu = \sigma_a \left( \sum_\nu W_{a,\nu}^\mu p_i^\nu + b_a^\mu \right) \quad (16)$$

where  $\theta(\cdot)$  is the step function and  $\sigma_a(\cdot)$  a nonlinear function.

### B.4 Diffusion and the SI Model as Reaction Diffusion

In regular diffusion on a graph, we have two states  $S, I$  and diffusion is changing the  $S \rightarrow I$  state. The probability  $P_{ij} \equiv P(x_i^{t+1} = I | x_j^t = S)$  of node  $i$  getting infected at  $t+1$ , given node  $j$  was in the infected state at time  $t$ , can be expressed in the form of is determined by the adjacency matrix  $A_{ij}$  because node  $j$  can only infect its neighbors. The infection probability is given by  $p_i^I(t+1) = \beta A_{ij} p_j^I(t)$  and  $p_i^S = 1 - p_i^I$ . Hence, for diffusion

$$f_1(x) = x \quad g_1(A) = \beta A, \quad h_1(p_j)^\mu = \sum_\nu \delta_\nu^\mu \delta_\nu^I p_j^\nu. \quad (17)$$

In regular diffusion there is no condition on the target node  $i$  and even if it is in the  $I$  state the dynamics is the same. In the SI model, however, the infection only spreads to  $i$  if it is in the  $S$  state. Thus, we have to multiply the dynamics by  $p_i^S \equiv P(x_i^t = S)$  which yields

$$p_i^I(t+1) = \beta A_{ij} p_j^I(t) p_i^S. \quad (18)$$

This can still be written as (9) by adding the extra functions

$$f_2(x) = x, \quad g_2(A) = I, \quad h_2(p_j)^\mu = \sum_\nu \delta_\nu^\mu \delta_\nu^S p_j^\nu \quad (19)$$

and having

$$p_i(t+1)^I = F_1(A; p(t))_i^I F_2(A; p(t))_i^S \quad (20)$$

where  $F_a = f_a(g_a \cdot h_a)$  are as in (14). More complex epidemic spreading models such as SIR and SEIR can also be written in a similar fashion. In SIR and SEIR the rest of the dynamic equations are linear and do not involve the the graph adjacency  $A$  at all, meaning  $g_a(A) = I$  in the rest of the equations.

### B.5 Discrete Time Agent-based SIR as a Reaction Diffusion System

The agent-based models (3) and (4), which correct for double-counting of infection from multiple neighbours, are sometimes written as

$$P(x_i^{t+1} = I | x_i^t = S) = 1 - (1 - \beta)^{\xi_i}, \quad (21)$$

where  $\xi_i$  is the total number of neighbors  $j$  of  $i$  which are infected, meaning  $x_j^t = I$ . We will first show that this is a special case of the form given in our paper. First, note that in (3) the terms can also be written as

$$(1 - \beta)^{\xi_i} = \prod_j \left( 1 - \beta \delta_{x_j^t, I} \right) \quad (22)$$

In the probabilistic model, we have to replace the strict condition of  $j$  being in the  $I$  state with its probability, so  $\delta_{x_j^t, I} \rightarrow P(x_j^t = I) = p_j^I(t)$ .

$$P(x_i^{t+1} = I | x_i^t = S) = 1 - \prod_{j \in \partial_i} \left( 1 - \beta \hat{A}_{ij} p_j^I \right) \quad (23)$$

and for small  $\beta$  yield

$$P(x_i^{t+1} = I | x_i^t = S) = \beta \sum_j \hat{A}_{ij} p_j^I - \beta^2 \sum_{j,k} \hat{A}_{ij} p_j^I \hat{A}_{ik} p_k^I + O(\beta^3) \quad (24)$$

which yields the simplified equation  $p_i(t+1)^I = p_i^S(t) \sum_j \beta \hat{A}_{ij} p_j^I(t)$ . Note that if the infection rate per time step  $\beta$  is large  $\beta \sum_j \hat{A}_{ij} p_j$  can exceed 1, rendering (24) inconsistent with  $p_i^I$  being probabilities. Both (23) and (24) both can be written in the form of RD (15) and (9). We utilize the  $h_1, g_1$  and  $h_2, g_2$  found for diffusion (17) and SI (19)

$$F_1(A; p)_i^\mu = \sum_j \log \left( 1 - \beta \hat{A}_{ij} h_1(p_j)^\mu \right) \quad F_1(A; p)_i^\mu = h_2(p_i)^\mu \quad (25)$$

and defining the probability as

$$\begin{aligned} p_i^I(t+1) &= F_1^S \left( 1 - \exp \left[ F_2^I \right] \right) = p_i^S(t) \left( 1 - \prod_j \left( 1 - \beta A_{ij} p_j^I(t) \right) \right) \\ &\approx \beta p_i^S(t) \sum_j A_{ij} p_j^I(t) \end{aligned} \quad (26)$$

## B.6 Graph Isomorphism and Ambiguity of Patient Zero

It may happen that the problem of finding P0 is unidentifiable when some nodes in the graph are identical. For instance, when  $G_I$  is a tree, if P0 is predicted to be a leaf, all leaves sharing the same parent are equally likely to be P0. In such cases, we need to assess the accuracy of our prediction modulo automorphisms  $\text{Aut}(G_I)$ . Finding  $\text{Aut}(G_I)$  is the Graph Isomorphism (GI) problem, which is in NP, but not known if it is NP-complete [28], with existing algorithm being at least exponential in  $N$  [29]. We choose to use a simpler heuristic inspired by the Weisfeiler-Lehman (WL) graph kernel [50, 41]. A simple measure for encoding the local structure of the graph is the number nodes  $n_i^{(l)}$  within a distance  $l$  from node  $i$ . We label each node by the sequence  $n_i = (n_i^{(1)}, \dots, n_i^{(l_{\max})})$ .  $n_i^{(1)}$  is the degree of node  $i$  and we have  $n_i^{(l)} = \theta(A_I^l) \mathbf{1}$  with  $A_I^l$  being the  $l$ th power of the adjacency matrix of the  $G_I$  and  $\theta(\cdot)$  the step function.

Figure 7 shows that on trees there are many equivalent nodes, even non-leaf nodes. However, the structure of contact networks where diseases spread is much more localized, similar to a ‘‘Random Geometric Graph’’ (RGG). Left of Figure 7 shows that on RGG, the level of node equivalence is far less, with most nodes being distinguishable. In general, we find non-tree graphs with sufficient randomness (e.g. RGG and random graphs), there are very few equivalent nodes in small graphs. Hence, we believe in realistic settings this ambiguity won’t play a major role in identifiability of P0.

## B.7 Proofs

**Proposition 3.** *Reaction-diffusion dynamics on graphs is structurally equivalent of the message-passing neural network ansatz.*

*Proof:* Analyzing the full stochastic model requires closely tracking the individual events and varies in each run. Hence, we will work with mean-field diffusion dynamics using transition probabilities, instead. Denoting  $p_i^\mu(t) \equiv P(x_i^t = \mu)$  of node  $i$  being in states such as  $\mu \in \{S, I, \dots, R\}$  at time  $t$ , a Markovian reaction-diffusion dynamics can be written as

$$p_i^\mu(t+1) = \sigma \left( \sum_j F(A_{ij} \cdot h(p_j)^\mu) \right), \quad h_a(p_i)^\mu = \sigma \left( \sum_\nu W_{a,\nu}^\mu p_i^\nu + b^\mu \right) \quad (27)$$

where  $A_{ij}^a = \theta(A_{ij}) f(A)_{ij}$  with  $\theta(\cdot)$  being the step function and  $\sigma(\cdot)$  a nonlinear function. To see this, note that RD processes on graphs involve a message-passing (MP) step (e.g. an infection signal coming from neighbors of a node), and a reaction step where messages of different states  $\mu$  passed to node  $i$  interact with each other

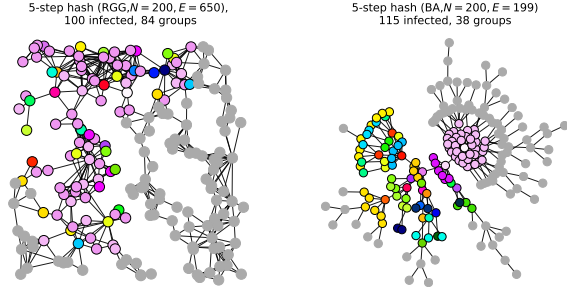


Figure 7: Equivalence classes of the quick hashing method inspired by WL. Grey nodes are outside  $G_I$ . The colors indicate the equivalence classes. On the tree (right)  $G_I$  has 115 nodes, but only 38 distinguishable groups. The Random Geometric Graph (left), however, with  $|G_I| = 100$  has 84 groups.

on node  $i$ . RD dynamics such as the SIR and SEIR models are also Markovian and the probability  $p_i^\mu(t)$  only depends on the probabilities at  $t - 1$ . These are also the conditions satisfied by MPNN. In (27),  $\mathcal{A}$  are a set of propagation rules for the messages, which are only nonzero where  $A$  is nonzero, same as the aggregation rule in MPNN. To have interactions between states  $\mu$  occurring inside each fixed node  $i$ ,  $h(p_i)$  can mix the states  $\mu$  but not change the node index  $i$ , leading to the form of  $h(p_i)$  in (27), which is the general ansatz for a neural network with weight sharing for nodes, same as in MPNN, and graph neural networks in general.  $\square$

**Proposition 4.** *In the worst case, after  $\tau$  steps of RD dynamics on a graph with diameter  $\text{Dia}(G)$ , we need  $l_{MP} > \min(\tau, \text{Dia}(G))$  layers of message-passing (MP) to be able to identify all P0.*

*Proof:* From (27), the MP step states that the state of node  $i$  at time  $t$  is only affected directly by its first neighbors at time  $t - 1$ . By induction, at  $t - \tau$  all nodes at most  $\tau$  steps away from  $i$  can have affected its state, meaning

$$p_i(t)^\mu = F_\tau(\{p_j^\nu(t - \tau) | \nu = S, \dots, R; A_{ij}^\tau \neq 0\}) \quad (28)$$

The  $j$  for which  $A_{ij}^\tau \neq 0$  are the nodes at most  $\tau$  steps away from  $i$ . Assuming  $G$  is connected, define the diameter of graph  $\text{Dia}(G) \equiv \min_l (A_{ij}^l \neq 0, \forall i, j)$ , i.e. the maximum shortest distance between any two nodes. Clearly, when  $\tau \geq \text{Dia}(G)$ , the state of any node will depend on all other nodes in the past and  $|G_I| = |G| = N$ . After  $\tau$  steps, P0 and the last infected nodes  $i$  can be a graph distance  $\tau$  apart. In the worst case, finding P0 requires the MP function  $p_{P0}$  calculated at node P0 to incorporate the last infected nodes. From (28), when  $l_{MP} < \tau < \text{Dia}(G)$ , with  $l_{MP}$  MP steps it is impossible for  $p_{P0}$  to become a function of a node  $i$  which is a distance of more than  $l_{MP}$  away. Hence we need at least  $\tau$  MP steps, unless  $\tau > \text{Dia}(G)$ , in which case we can go from any node to any other with  $l_{MP} = \text{Dia}(G)$  MP steps.  $\square$

## B.8 Accuracy Drop and $t_{\max}$

### B.8.1 Proof of Theorem 1

*Proof:* To show this we will establish bounds on the cycles the contagion may encounter on a connected ER graph. Let  $G_I$  be the subgraph of  $G$  to which the epidemic has spread, which includes all nodes in the  $I$  and  $R$  states. ER graphs are known to be locally tree-like, because the probability of three connected nodes to make a triangle is  $c = \binom{N}{3} p^3 / \binom{N}{3} p^2 = p$ , same as edge probability. Using (2), being locally tree-like means descendent nodes are likely not yet infected, allowing the exponential growth to persist until  $|G_I| \sim O(N)$ . However, the exponential growth of  $\sum_i I_i(t)$  in (2) leads to a depletion of susceptible nodes and a slow-down of the epidemic. In fact, a logistic curve is a good approximation of the  $\sum_i S_i(t) \approx \sigma[\gamma(R_0 - 1)(t - t_{\max})]$ , because in (1) when  $R_i \approx 0$ ,  $dS_i/dt \approx \beta A_{ij}(1 - S_i)S_i$ , which is a logistic equation. When  $t < t_{\max}$ , the logistic function is exponential, as in (2), and it slows down when an  $O(1)$  fraction of nodes are infected, or  $|G_I| \sim O(1)N$ . Setting  $\sum_i I_i(t_{\max}) + R_i(t_{\max}) \sim O(1)N$  in (2), we get  $t_{\max} \sim \log N / (\beta\lambda_1 - \gamma)$ , since  $\log O(1) \sim 0$ . Plugging in  $R_0 = \beta\lambda_1/\gamma$ , we obtain (6).  $\square$

### B.8.2 Proof of Theorem 2 $P_{tri}$

*Proof:* If P0 is in a triangle, we may miss it 2/3 of the times. Thus, the probability of detecting P0 is bounded by  $P < 1 - P_{tri} \times 2/3$ , where  $P_{tri}$  is the probability that P0 is in a triangle. Since edges in  $G$  are uncorrelated, each having probability  $p$ ,  $G_I$  is also a connected random graph with the same edge probability  $p$ . Hence, in  $G_I$  all nodes have degree  $k \approx p|G_I|$ .  $P_{tri}$  is one minus the probability that none of the  $k$  neighbors of P0 are connected, i.e.  $P_{tri} = 1 - (1 - p)^{\binom{G_I}{2} p}$ , which proves the proposition.  $\square$

## C Covid-19 Data and Simulations

**Geolocation data** Mobility data are provided by Cuebiq, a location intelligence and measurement platform. Through its Data for Good program (<https://www.cuebiq.com/about/data-for-good/>), Cuebiq provides access to aggregated and privacy-enhanced mobility data for academic research and humanitarian initiatives. These first-party data are collected from users who have opted in to provide access to their GPS location data anonymously, through a GDPR-compliant framework. Additionally, Cuebiq provides an estimate of home

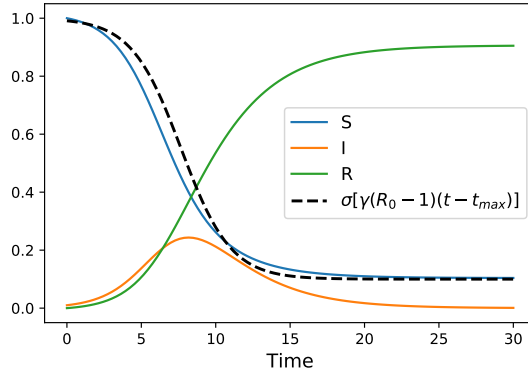


Figure 8: A logistic curve around the predicted  $t_{\max}$  yields a good fit for the behavior of  $\sum_i S_i(t)$ .



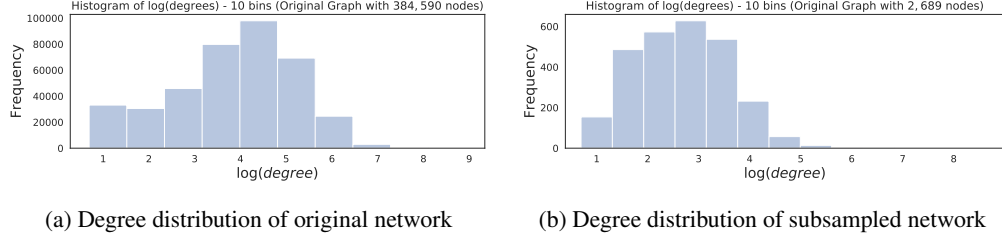


Figure 9: Degree distribution of the original co-location network with 384,590 nodes and the subsampled network with 2,689 nodes. We subsample the larger network to find a subgraph in order to reduce computational costs of our experiments. We observe that the distribution of our subsampled network is similar to the original graph.

and work census areas for each user. In order to preserve privacy, noise is added to these “personal areas”, by upleveling these areas to the Census block group level. This allows for demographic analysis while obfuscating the true home location of anonymous users and preventing misuse of data.

**Colocation network** The method for constructing the co-location graphs is as follows. First, we split each day into five minute time windows, resulting in 288 time bins per day. For every location event, we use its timestamp to assign it to a time bin, then assign the longitude-latitude coordinate of the observation to an 8-character string known as a *geohash*. A geohash defines an approximate grid covering the earth, the area of which varies with latitude. The largest dimensions of an 8-character geohash are 38m x 19m, at the equator. If a user does not have an observation for a given time bin, we carry the last observation forward until there is another observation. We finally define two users to be co-located — and therefore to have a timestamped edge in the graph — if they are observed in the same geohash in the same time bin. Accordingly, our co-location graph is constructed by observing the greater Boston area over two weeks from 23 March, 2020 to 5 April, 2020 and results in a graph with  $N = 384,590$  nodes. To reduce computational costs, we sample a subgraph with  $N = 2,689$  nodes and  $|E| = 30,376$  edges with similar degree distribution and connectivity patterns as the original graph and can be observed in Fig 9.

**Epidemic simulations in real data.** We run a SEIR model on the real co-location network. In doing so, we select parameters and modify the structure of the model to resemble the natural history of COVID-19 [7]. At each time step nodes, according to their health status, can be in one of five compartments:  $S$ ,  $E$ ,  $I$ ,  $I_a$ , or  $R$ . Thus, we split infectious nodes in two categories. Those that are symptomatic ( $I$ ) and those that are asymptomatic ( $I_a$ ). The first category infects susceptible node, with probability  $\lambda$  per contact. The second category instead with probability  $r_a \lambda$ . We set  $r_a = 0.5$  and consider that probability of becoming asymptomatic as  $p_a = 0.5$ . The generation time, that is the sum of incubation ( $\alpha^{-1}$ ) and infectious period ( $\gamma^{-1}$ ), is set to be 6.5 days. Specifically, we fix  $\alpha^{-1} = 2.5$  and  $\gamma^{-1} = 4$  days. In a single, homogeneously mixed, population the basic reproductive number of such epidemic model is  $R_0 = (1 - p_a + r_a p_a) \beta / \gamma$  where  $\beta$  is the per capita spreading rate [17]. Here however, the epidemic model unfolds on top of the real co-location network. Hence, infected nodes are able to transmit the disease only via contacts (with susceptible individuals) established during the observation period. As mentioned above, the value of  $R_0$  is defined by the interplay between the disease’s parameters as well as the structural properties of the network [35, 26]. For simplicity we approximate  $\beta = \langle k \rangle \lambda$ , where  $\langle k \rangle$  is the average number of connections in the network. We obtain  $\lambda = 0.073$  after solving for  $R_0$  and plugging in  $\langle k \rangle = 30376/2689 = 11.29$ . The simulations start with an initial infectious seed selected uniformly at random among all nodes. We then read and store the time-aggregated network in memory. The infection dynamics, which are catalysed by the contacts between infectious and nodes, take place on such network. The spontaneous transitions instead (i.e. transition from  $S$  to  $E$  and the recovery process), take place independently of the connectivity patterns. After the infection and recovery dynamics, we print out the status, with respect to the disease, of each node. Finally, we create a dataset with 10,000 samples and an 80 – 10 – 10 train-validation-test split.